

Determination of Intrinsic Ferroelectric Polarization in Orthorhombic Manganites with E-type Spin Order

Y. S. Chai,¹ Y. S. Oh,¹ L. J. Wang,² N. Manivannan,¹ S. M. Feng,² Y. S. Yang,¹ L. Q. Yan,¹ C. Q. Jin,² and Kee Hoon Kim^{1,*}

¹*CeNSCMR, Department of Physics and Astronomy, Seoul National University, Seoul 151-742, Republic of Korea*

²*Institute of Physics, Chinese Academy of Science, P. O. Box 603, Beijing 100080, P. R. China*

By directly measuring electrical hysteresis loops using the Positive-Up Negative-Down (PUND) method, we accurately determined the remanent ferroelectric polarization P_r of orthorhombic $RMnO_3$ ($R = Ho, Tm, Yb, \text{ and } Lu$) compounds below their E-type spin ordering temperatures. We found that $LuMnO_3$ has the largest P_r of $0.17 \mu C/cm^2$ at 6 K in the series, indicating that its single-crystal form can produce a P_r of at least $0.6 \mu C/cm^2$ at 0 K. Furthermore, at a fixed temperature, P_r decreases systematically with increasing rare earth ion radius from $R = Lu$ to Ho , exhibiting a strong correlation with the variations in the in-plane Mn–O–Mn bond angle and Mn–O distances. Our experimental results suggest that the contribution of the Mn t_{2g} orbitals dominates the ferroelectric polarization.

PACS numbers: 75.85.+t, 77.80.-e, 75.50.Ee, 75.47.Lx

*khkim@phya.snu.ac.kr

Recent intensive researches on multiferroic materials are motivated by great interests in the fundamental physics of spin-lattice coupling as well as the potential for using these materials in the multifunctional memories and sensors.¹⁻⁴ An interesting class of multiferroic materials that have been studied intensively in recent years is the so-called magnetic ferroelectrics. In these materials, the ferroelectric polarization (P), induced by the primary magnetic order, can be sensitively tuned by magnetic fields through the control of magnetic states.⁵ It is now well-known that both collinear and non-collinear spin orderings in these magnetic ferroelectrics can generate a nontrivial P through several mechanisms such as exchange-striction^{6,7} and the inverse Dzyaloshinskii–Moriya interaction.^{8,9} Limited by the rather weak spin-lattice coupling strength set by these mechanisms, most of the magnetic ferroelectrics studied so far exhibit P values less than $0.1 \mu\text{C}/\text{cm}^2$, which is much smaller than that of conventional ferroelectrics.

On the other hand, several theoretical works have suggested the possibility of achieving large P in orthorhombic (o)- RMnO_3 ($R = \text{Ho, Er, Tm, Yb, and Lu}$) with a collinear E-type antiferromagnetic (AFM) spin order.¹⁰⁻¹³ In this system, Mn^{3+} has a $t_{2g}^3 e_g^1$ configuration and thus undergoes an e_g orbital ordering with the Jahn–Teller distortion of the MnO_6 octahedra, leading to a distribution of long and short Mn–O bond lengths (d_l and d_s) in the ab -plane [Fig. 1(a)].¹⁴ The E-type AFM order at low temperatures is predicted to induce P by two different mechanisms. First, the ionic displacement polarization P_{ion} is induced by the competition between the ferromagnetic super-exchange interaction between e_g orbitals and the AFM interaction between t_{2g} orbitals through the inverse Goodenough–Kanamori rules,^{10,11} as illustrated in Fig. 1(b). Second, the electronic polarization P_{ele} results from selective electron hopping between orbitals with parallel spins and has contributions from both t_{2g} and e_g orbitals as well as oxygen, although the t_{2g} and e_g

orbital contributions nearly cancel each other, leaving just mainly the O contribution in the end. As summarized in Fig. 1(b),¹⁰ the t_{2g} and e_g contributions in both mechanisms have opposite signs and the total P results from the sum of those contributions. Both model Hamiltonian¹² and first-principles¹⁰ calculations predicted that a total P up to approximately $6 \mu\text{C}/\text{cm}^2$ can be obtained in o -HoMnO₃ and the value is almost same over the o -RMnO₃ series (from $R = \text{Ho}$ to Lu). In a subsequent study using the hybrid functional approach, the predicted value decreased to approximately $2 \mu\text{C}/\text{cm}^2$. This reduction occurred because the hybrid functional method reduces the electronic contribution.¹⁵

An experimental test of these theoretical results is an important and necessary step in multiferroic research as it can not only identify the maximum allowed P when the E-type spin order is present but may also help find yet another new compound generating large P . However, previous experimental studies on the o -RMnO₃ compounds have shown inconsistent results. Early studies on o -HoMnO₃ and o -TmMnO₃ revealed P values inside the E-type AFM phase of approximately $0.008 \mu\text{C}/\text{cm}^2$ at 5 K and $0.15 \mu\text{C}/\text{cm}^2$ at 2 K.^{17,18} More recently, P values of 0.07 – $0.09 \mu\text{C}/\text{cm}^2$ were observed at 2 K for all o -RMnO₃ ($R = \text{Ho}, \text{Tm}, \text{Yb}, \text{Lu},$ and $\text{Y}_{1-y}\text{Lu}_y, y = 0-1$), which changed little with variation in the rare earth ion radius (r_R).¹⁹ It should be noted that all of these previous reports employed the pyroelectric current (J_p) measurement. In this method, the temperature-dependent J_p is measured upon warming after applying dc electric poling from a high temperature above the ferroelectric Curie temperature to the low temperature at which the measurement starts. The temperature dependent polarization $P_{\text{dc}}(T)$ can be attained by integrating J_p as a function of time. However, the common procedures followed in this method turned out to provide inaccurate P data due to several experimental challenges. First, most of the o -RMnO₃ ($R =$

Ho to Lu) compounds have a polycrystalline pellet form synthesized under a high pressure. Because of this, the J_p measurement is subject to incomplete electric poling and thus the ferroelectric domains can be randomly oriented. Second, the electric poling process usually produces space charges that can be trapped at the polycrystalline grain boundaries, providing a spurious P contribution. These fundamental challenges in determining the P value in polycrystalline ferroelectrics can be greatly reduced by employing the so-called Positive-Up Negative-Down (PUND) method,²⁰ which has been extensively employed in ferroelectric thin film researches and recently has been applied to multiferroic single crystals.²¹ In particular, we have recently used this technique to prove that a polycrystalline o -HoMnO₃ sample has an intrinsic P of approximately $0.24 \mu\text{C}/\text{cm}^2$,²² which is much smaller than that predicted by band calculations.^{10,12,15}

In this communication, we report our systematic efforts to determine the intrinsic ferroelectric polarization of o -RMnO₃ for $R = \text{Ho, Tm, Yb, and Lu}$ with E-type spin order. By applying the PUND method to high quality specimens that have been well characterized by structural studies, we succeeded in measuring electrical hysteresis loops for all the samples as a function of temperature. We found that the remanent ferroelectric polarization P_r systematically increases with decreasing r_R and thus o -LuMnO₃ (HoMnO₃) produces the largest (smallest) P_r value of 0.17 (0.068) $\mu\text{C}/\text{cm}^2$ at 6 K. Based on the local structure analysis, we suggest that the orthorhombic manganites with E-type spin order have higher electronic polarization contributions from the t_{2g} than the e_g orbitals.

o -RMnO₃ ($R = \text{Ho, Er, Tm, Yb, and Lu}$) specimens were synthesized under a high pressure of 5 GPa at 1423 K²³ and an X-ray diffraction study confirmed the orthorhombic ($Pbnm$) structure at

300 K was free of impurities. Crystal structures were extracted by Rietveld refinement using the GSAS program. All the specimens investigated for the hysteresis loop had a density at least 95% of their theoretical value. We made thin plate-like samples with thickness of approximately 0.3 mm, used silver epoxy (EPTEK H20E) to make electrodes. We employed a PPMSTM (Quantum Design) to control temperature environment for the hysteresis loop or J_p measurements. For the PUND method, we applied a series of positive (P_i , $i = 0-2$) and negative (N_i , $i = 0-2$) electric pulses as shown in Fig. 2(a). The first two pulses, P0 and N0, are used to fully align the ferroelectric domains. During the next two pulses, P1 and P2 (N1 and N2), two curves representing effective polarization changes are recorded in the Sawyer–Tower circuit, and they are subtracted to form the half loop for electric field $E > 0$ ($E < 0$) [Fig. 2(b)]. As a result, the pure hysteretic parts of the hysteresis loop can be obtained without being obscured by resistive or capacitive components. Moreover, by employing a short pulse, the maximum peak field for electric poling can be increased to better align the ferroelectric domains without inducing electrical break-down effects. In particular, the space charge effect is minimized as the sample is poled in isothermal conditions. These features enable us to mitigate the experimental problems encountered in conventional J_p measurements with dc field poling.

Figure 2(c) displays a typical electrical hysteresis loop obtained by this procedure, for the case of *o*-LuMnO₃ at 6 K. The y -axis offset directly represents $P_r \approx 0.17 \mu\text{C}/\text{cm}^2$. At each temperature, we have measured the loop by increasing amplitude of the pulse and then determined the polarization until the electrical break-down happens. The P_r vs. maximum E curves thus obtained for *o*-LuMnO₃ at 15 K and 25 K show almost saturation at the high field, suggesting that P_r at the maximum E of 11.8 MV/m is close to the intrinsic polarization due to fully aligned ferroelectric

domains. To verify thus obtained P_r value by the PUND method, the pyroelectric current J_p has been also measured after the short N₂ pulse [Fig. 2(a)], and the temperature dependence of P , termed as $P_{\text{pls}}(T)$ in Fig. 2(c), has been estimated. The difference between P_r and $P_{\text{pls}}(T)$ turns out to be less than 5% at 6 K, supporting the conclusion that both P_r and $P_{\text{pls}}(T)$ are close to the intrinsic ferroelectric polarization. However, the $P_{\text{dc}}(T)$ curves determined through the J_p measurement after dc electric field poling did not show saturation before an electrical break-down. Moreover, the maximum polarization values obtained at both 15 K and 25 K were clearly larger than those obtained using the PUND method. It is most likely that the conventional $P_{\text{dc}}(T)$ measurements include significant contributions from trapped space charges that have accumulated during the poling process, while the $P_{\text{pls}}(T)$ measurements do not.

By applying the same experimental method, we determined the electrical hysteresis loops at various temperatures for all the o - RMnO_3 ($R = \text{Ho, Tm, Yb, and Lu}$) after cooling the samples without an electric field bias [Figs. 3(a)–3(d)], and summarized the resultant temperature-dependence of P_r and the $P_{\text{pls}}(T)$ curves [Figs. 3(e)–3(h)]. The onset temperatures of ferroelectric polarization were found to be 26, 35, 37, and 38 K for $R = \text{Ho, Tm, Yb, and Lu}$, respectively and they are consistent with the reported lock-in transition temperature, T_L , in each compound.^{14,18,22,23} Surprisingly, o - LuMnO_3 clearly showed the largest P_r value of $0.17 \mu\text{C}/\text{cm}^2$ at 6 K and upon extrapolation, P_r would reach approximately $0.2 \mu\text{C}/\text{cm}^2$ at 0 K [Fig. 3(d)]. Because the E-type spin order is supposed to generate uniaxial electric polarization along the a -axis, we can expect that a polycrystalline specimen would have roughly one third of the single crystal polarization value because of the random orientation of grains. Therefore, $P_r = 0.2 \mu\text{C}/\text{cm}^2$ in our polycrystalline sample predicts at least $P_a = 0.6 \mu\text{C}/\text{cm}^2$ in the o - LuMnO_3 single crystal. We note

that this P_a value is significantly larger than those observed in typical magnetic ferroelectrics although it is still much lower than the theoretically predicted values of approximately 2–6 $\mu\text{C}/\text{cm}^2$.^{10,15}

It is uniquely revealed in our investigations that the ferroelectric polarization in the studied orthorhombic manganites systematically changes with the variation in r_R . Figure 3 shows that with the decrease in r_R from o -HoMnO₃ to o -LuMnO₃, P_r values increase systematically over all temperatures. Figure 4(a) summarizes the $3P_r$ vs. r_R relationship at temperatures of 6 K and $T_L/2$ (= 13, 17.5, 18.5, and 19 K for $R = \text{Ho, Tm, Yb, and Lu}$, respectively), proving that the $3P_r$ values increase when the r_R is reduced. Upon comparing those $3P_r$ values of o -HoMnO₃ and o -LuMnO₃, we find that the $3P_r$ values increase by 1.2 and 0.67 times at 6 K and $T_L/2$, respectively. Because the hysteresis loops at $T_L/2$ are clearly saturated at high E while the loops at 6 K are less saturated, the smoothly increasing tendency observed at $T_L/2$ should reflect the intrinsic r_R dependence. We note that our observations are in contrast with the theoretical results in Ref. 10, which predicts an almost constant P behavior regardless of r_R changes. Furthermore, our results are also inconsistent with the experimental data in Ref. 19, in which the J_p measurements subject to the trapped space charge problems resulted in P values that were almost constant over different r_R . We also note that different annealing treatments under O₂, N₂, and air atmospheres in our o -HoMnO₃ specimen did not show any significant changes in the P_r vs. temperature curves,²² suggesting that the observed r_R dependence is rather insensitive to oxygen stoichiometry in the o -RMnO₃ specimens. Therefore, it is likely that the current $3P_r$ vs. r_R data reflect the intrinsic polarization behavior in o -RMnO₃ ($R = \text{Ho, Tm, Yb, and Lu}$).

In order to understand the origin of this rather clear change of P_r with r_R , we determined the

structural parameters of the samples at 300 K and the results are summarized in Figs. 4(b) and 4(c). The resultant lattice constants and in-plane Mn–O–Mn bond angle ϕ are quite similar to the reported experimental values.²³ Indeed, the ϕ value systematically decreases with r_R , showing that the compounds with a smaller r_R result in a more distorted local structure. On the other hand, the Mn–O bond lengths, d_l and d_s , clearly show opposite tendency with the variation in r_R ; d_l (d_s) increases (decreases) with the decrease in r_R [Fig. 4(c)]. This experimental finding is consistent with other experiment results²³ but is in contrast with the behavior of the input parameters used in the first principles calculation,¹⁰ in which the optimized crystal structure in the E-type spin order results in the decreasing behaviors for both d_l and d_s with decreasing r_R . Figure 4(c) compares these contrasting experimental and theoretical behaviors of d_l and d_s with r_R . Moreover, we note that the experimental changes of d_l and d_s over r_R , which turn out to be approximately 3%, are much bigger than the theoretical predictions, which are less than 0.5%. These lattice parameter variations over r_R are thus expected to hold even at low temperatures because thermal shrinking in these *o*-RMnO₃ compounds is estimated to be less than 0.3% between 300 and 10 K.¹⁸

The first principles calculation in Ref. 10 discussed how the input structural parameters can crucially affect the electronic polarization P_{ele} , which is dominant over the ionic polarization, P_{ion} . Firstly, with decreasing d_l , the hopping integral between the e_g orbitals increases and thus the e_g contribution to P_{ele} increases. Secondly, the decrease of d_s can enhance the hopping between t_{2g} orbitals so that the t_{2g} contribution to P_{ele} will increase too. Because the enhanced contributions of e_g and t_{2g} orbitals are opposite in sign, the total P should eventually become almost independent of r_R and then become close to $6 \mu\text{C}/\text{cm}^2$ in all the *o*-RMnO₃ ($R = \text{Ho to Lu}$).¹⁰ The dashed lines in Fig. 4(d) schematically describe these theoretical predictions for the hopping integrals and related

contributions to P_{ele} .

On the other hand, our new experimental results for d_t and d_s in Fig. 4(c) suggest a new scenario that with decreasing r_R , the hopping integral between e_g orbitals should be suppressed significantly while that between t_{2g} orbitals should be increased [solid lines in Fig. 4(d)]. Accordingly, we can expect that the t_{2g} orbitals contribute to P_{ele} more significantly than e_g orbitals overall, and this tendency would increase more as R changes from Ho to Lu [Fig. 4(d)]. As the ionic and oxygen contributions were relatively small and nearly independent of r_R , the total P would be then enhanced in proportion to P_{ele} . The observed increase of $3P_r$ from o -HoMnO₃ to o -LuMnO₃ seems consistent with this qualitative explanation based on the existing theoretical prediction. It will be worth further theoretical investigation based on the structural and electrical informations provided here to see whether the existing theoretical framework is still valid or requires other explanations to understand the intrinsic polarization value and its rare earth dependence in o -RMnO₃.

To conclude, we determined the intrinsic ferroelectric polarization in o -RMnO₃ ($R = \text{Ho, Tm, Yb, and Lu}$) with E-type spin order by using the PUND method. The obtained polarization values increase systematically upon reducing the rare earth ionic radius from $R = \text{Ho}$ to Lu, and the maximum ferroelectric polarization value at 0 K is estimated to be approximately $0.6 \mu\text{C}/\text{cm}^2$ in o -LuMnO₃. Our structural analyses imply that t_{2g} rather than e_g orbitals play a more crucial role in determining ferroelectric polarization.

We thank Y. Liu for helpful discussion. This work was financially supported by the National Creative Research Initiative (2010-0018300) and the Fundamental R&D Program for Core Technology of Materials of MOKE.

References

- ¹T. Kimura, N. Goto, H. Shintani, T. Arima and Y. Tokura, *Nature (London)* **426**, 55 (2003).
- ²N. Hur, S. Park, P. A. Sharma, J. S. Ahn, S. Guha and S.-W. Cheong, *Nature (London)* **429**, 392 (2004).
- ³M. Fiebig, *J. Phys. D* **38**, R123 (2005).
- ⁴D. I. Khomskii, *J. Magn. Magn. Mater.* **306**, 1 (2006).
- ⁵S.-W. Cheong and M. Mostovoy, *Nature Mater.* **6**, 13 (2007).
- ⁶L. C. Chapon, G. R. Blake, M. J. Gutmann, S. Park, N. Hur, P. G. Radaelli and S. -W. Cheong, *Phys. Rev. Lett.* **93**, 177402 (2004).
- ⁷Y. J. Choi, H. T. Yi, S. Lee, Q. Huang, V. Kiryukhin and S. -W. Cheong, *Phys. Rev. Lett.* **100** 047601 (2006).
- ⁸M. Kenzelmann , A. B. Harris, S. Jonas, C. Broholm, J. Schefer, S. B. Kim, C. L. Zhang, S.-W. Cheong, O. P. Vajk and J. W. Lynn, *Phys. Rev. Lett.* **95**, 087206 (2005).
- ⁹T. Arima, A. Tokunaga, T. Goto, H. Kimura, Y. Noda and Y. Tokura, *Phys. Rev. Lett.* **96**, 097202 (2006).
- ¹⁰K. Yamauchi, F. Freimuth, S. Blugel and S. Picozzi, *Phys. Rev. B* **78**, 014403 (2008).
- ¹¹K. Yamauchi and S. Picozzi, *J. Phys. Condens. Mat.* **21**, 064203 (2009).
- ¹²I. A. Sergienko, C. Sen and E. Dagotto, *Phys. Rev. Lett.* **97**, 227204 (2006).
- ¹³S. Picozzi, K. Yamauchi, B. Sanyal, I. A. Sergienko and E. Dagotto, *Phys. Rev. Lett.* **99**, 227201 (2007).
- ¹⁴Y. Murakami, J. P. Hill, D. Gibbs, M. Blume, I. Koyama, M. Tanaka, H. Kawata, T. Arima, Y. Tokura, K. Hirota and Y. Endoh, *Phys. Rev. Lett.* **81**, 582 (1998).

- ¹⁵A. Stroppa and S. Picozzi, *Phys. Chem. Chem. Phys.* **12**, 5405 (2010).
- ¹⁶S. Picozzi, K. Yamauchi, G. Bihlmayer and S. Blügel, *Phys. Rev. B* **74**, 094402 (2006).
- ¹⁷B. Lorenz, Y. Q. Wang and C. W. Chu, *Phys. Rev. B* **76**, 104405 (2007).
- ¹⁸V. Yu. Pomjakushin, M. Kenzelmann, A. Dönni, A. B. Harris, T. Nakajima, S. Mitsuda, M. Tachibana, L. Keller, J. Mesot, H. Kitazawa and E. T.-Muromachi, *New J. Phys.* **11**, 043019 (2009).
- ¹⁹S. Ishiwata, Y. Kaneko, Y. Tokunaga, Y. Taguchi, T. Arima and Y. Tokura, *Phys. Rev. B* **81**, 100411(R) (2010).
- ²⁰J. F. Scott, L. Kammerdiner, M. Parris, S. Traynor, V. Ottenbacher, A. Shawabkeh and W. F. Oliver, *J. Appl. Phys.* **64**, 787 (1988).
- ²¹M. Fukunaga and Y. Noda, *J. Phys. Soc. Jpn.* **77**, 064706 (2008).
- ²²S. M. Feng, Y. S. Chai, J. L. Zhu, N. Manivannan, Y. S. Oh, L. J. Wang, Y. S. Yang, C. Q. Jin and Kee Hoon Kim, *New J. Phys.* **12**, 073006 (2010).
- ²³M. Tachibana, T. Shimoyama, H. Kawaji, T. Atake, and E. T.-Muromachi, *Phys. Rev. B* **75**, 144425 (2007).

Figure Captions:

FIG. 1. (a) ab -plane arrangement of Mn and O atoms and spins in the E-type spin order realized in o -RMnO₃. (b) The arrows represent the O atom displacement due to e_g (solid) and t_{2g} (dashed) orbitals. (c) The ellipses indicate the Mn charge deviations due to the e_g (along d_l) and t_{2g} (along d_s) hoppings, as described in Ref. 10. Arrows at the bottom depict the resultant polarizations from each contribution categorized into P_{ion} and P_{ele} .

FIG. 2. (a) Electrical pulse patterns used in the PUND method. (b) The schematic view to extract the hysteresis loop out of the pulse sequences in (a). (c) Typical hysteresis loop at 6 K and (d) $P_{\text{pls}}(T)$ after the N2 pulse. (e) Remanent polarization P_r vs. peak electric field E applied at 15 and 25 K for o -LuMnO₃. Polarization values (at 15 and 25 K) obtained by the conventional pyroelectric current measurements after dc electric field poling, $P_{\text{dc}}(T)$, are also plotted as a function of applied dc electric field.

FIG. 3. Electrical hysteresis loops of (a) o -HoMnO₃, (b) o -TmMnO₃, (c) o -YbMnO₃, and (d) o -LuMnO₃. Remanent polarization P_r values and related $P_{\text{pls}}(T)$ curve are summarized in (e)–(h). The data in (e) are reproduced from Ref. 22.

FIG. 4. The rare earth ionic radius r_R dependence for (a) $3P_r$ values at 6 K and $T_L/2$, (b) lattice constants and bond angle (ϕ), and (c) experimental d_s and d_l (solid symbols) at room temperature and calculated average d_s and d_l (open symbols) (from Ref. 10). (d) Schematic diagram for expected hopping integrals for t_{2g} (top panel) and e_g (middle panel) orbitals, and related electronic polarization contributions (bottom panel). Solid and dash lines represent the expected contributions from experimental and calculated data.

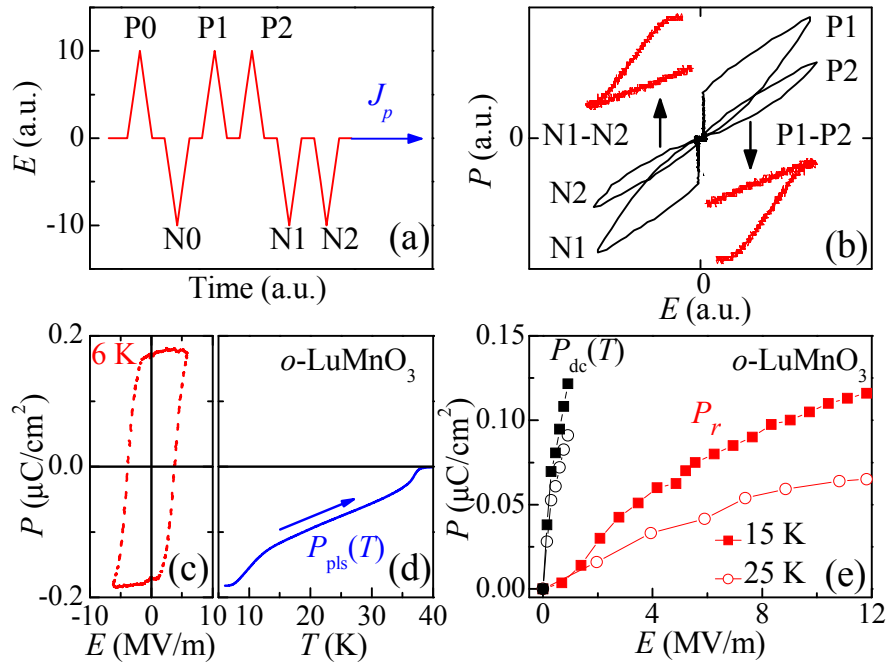


Figure 2

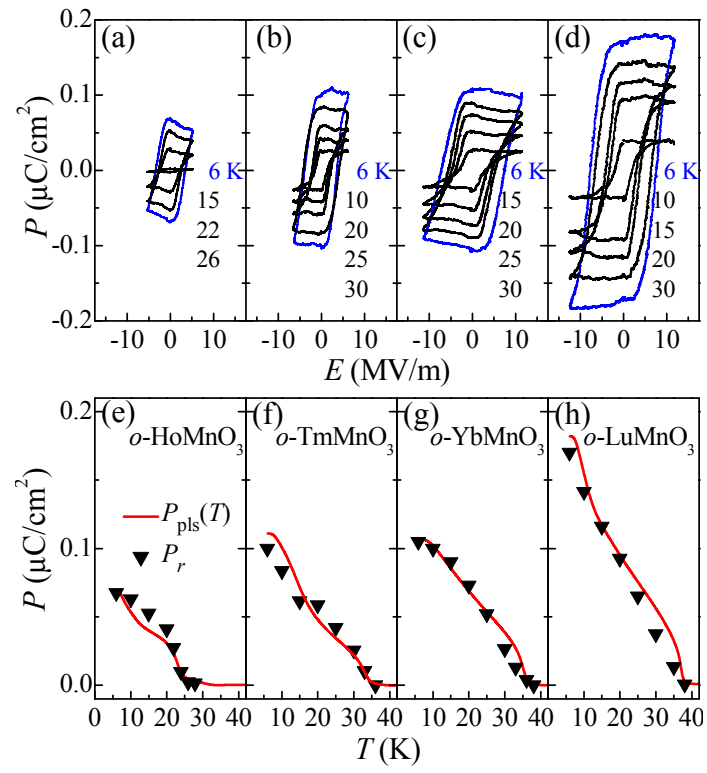


Figure 3

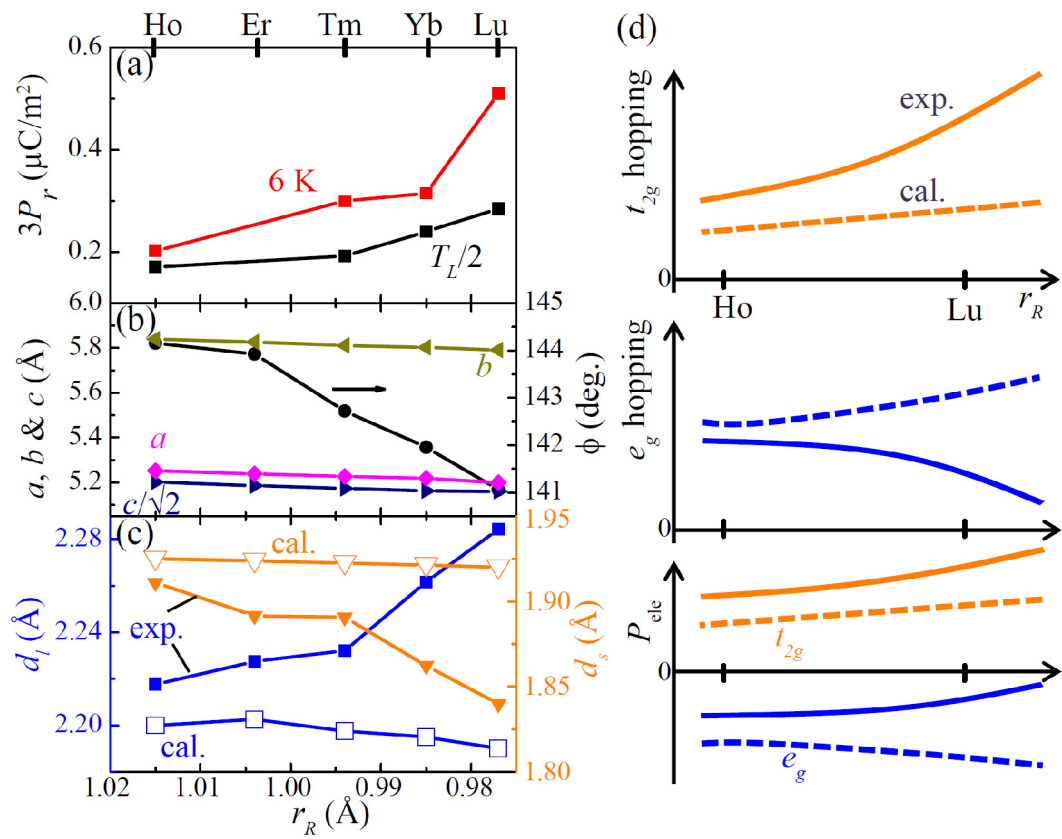


Figure 4